# Adiabatic-limit Coulomb factors for photoelectron and high-order-harmonic spectra

M. V. Frolov, N. L. Manakov, A. A. Minina, S. V. Popruzhenko, and Anthony F. Starace

Phys. Rev. A **96**, 023406 — Published 4 August 2017

DOI: 10.1103/PhysRevA.96.023406

# Adiabatic Limit Coulomb Factors for Photoelectron and High-order Harmonic Spectra

M. V. Frolov,[1] N. L. Manakov,[1] A. A. Minina,[1] S. V. Popruzhenko,[1,2,3] and Anthony F. Starace[4]

[1] *Department of Physics, Voronezh State University, Voronezh 394018, Russia*
[2] *Max-Planck Institut für Physik komplexer Systeme, Dresden 01187, Germany*
[3] *National Research Nuclear University "MEPhI", Moscow 115409, Russia*
[4] *Department of Physics and Astronomy, The University of Nebraska, Lincoln, Nebraska 68588-0299, USA*

(Dated: July 5, 2017)

A momentum-dependent Coulomb factor in the probability for nonlinear ionization of atoms by a strong low-frequency laser field is calculated analytically in the adiabatic approximation. Expressions for this Coulomb factor, valid for an arbitrary laser pulse waveform, are obtained and analyzed in detail for the cases of linear and circular polarizations. The dependence of the Coulomb factor on the photoelectron momentum is shown to be significant in both cases. Using a similar technique, the Coulomb factor for emission of high-order harmonics by an atom in a bichromatic laser field is also calculated. In contrast to the case of a single-frequency field, for bichromatic fields the Coulomb factor depends significantly on the harmonic energy.

PACS numbers: 02.30.Mv, 03.65.Xp, 32.80.Wr

## I. INTRODUCTION

Above-threshold ionization (ATI) and high-order harmonic generation (HHG) resulting from the interaction of intense laser radiation with atomic and molecular systems have remained the focus of strong field physics for more than two decades. Furthermore, interest in these phenomena shows no signs of saturation, for at least two reasons. First, the highly nonlinear time-dependent dynamics of laser-driven atoms and molecules has continued to produce new effects, most of which are first observed experimentally and only later are explained theoretically. The last decade has been particularly fruitful, witnessing such "ionization surprises" [1] as the discovery of several types of low energy structures [2–5], photoelectron holography [6], and a low-energy plateau [7]. Second, HHG opens a means to generate extremely short and relatively bright pulses of UV and soft X-ray light using compact and economical setups [8–10]. Someday HHG-based table-top light sources will achieve intensities sufficient for a variety of practical applications. For particular applications, tailored laser pulses enable one to control the spectral and polarization properties of high-order harmonics. Moreover, the emerging new area of attosecond physics [11] is based on HHG.

These experimental advances require theory for their interpretation. The strong-field approximation (SFA) remains an important computational tool for theory (for reviews, see Refs. [12–15]). Its remarkable success is based on its combination of analytic simplicity and predictive power. Indeed, the celebrated Lewenstein model of HHG [16] is essentially based on the SFA. However, since the SFA in its standard form disregards the Coulomb interaction between a photoelectron and its parent ion, for neutral atoms and positively-charged ions the SFA is at best only qualitatively accurate. As experiments probe ever deeper into details of ATI and HHG processes, the SFA becomes increasingly insufficient for their description. In fact, all of the aforementioned "ionization surprises" are out of reach of this otherwise very fruitful method.

This paper has two aims. First, using the general approach of the so-called Coulomb-corrected SFA (CCSFA) [14, 17], we calculate analytically the momentum-dependent Coulomb factor in the ionization probability in the adiabatic limit, $\gamma \ll 1$ (where $\gamma$ is the Keldysh parameter [18]), and analyze it for the cases of linearly-polarized (LP) and circularly-polarized (CP) monochromatic fields. This result fills the gap between the static (momentum-independent) Coulomb factor responsible for enhancement of the ionization rate [19, 20] and the one for arbitrary $\gamma$, which can only be calculated numerically and which requires a demanding analysis of those trajectories that revisit the atom. Second, we use the adiabatic approximation to calculate Coulomb factors for HHG spectra produced by a bicircular laser field with a frequency ratio of 1:2. This second aim is motivated by the growing interest, both experimental [21–23] and theoretical [24–27], in HHG spectra produced by bicircular fields.

In Sec. II we provide a brief overview of theoretical methods for treating strong field processes in order to provide a context for the present work. In Sec. III we introduce the Coulomb-free SFA detachment amplitude and its representation in terms of saddle points and trajectories. We also derive approximate expressions for the saddle-point solutions and for the classical photoelectron action in the adiabatic limit. In Sec. IV we derive the Coulomb correction and analyze it for LP and CP fields. In Sec. V the adiabatic Coulomb correction for HHG spectra in bicircular laser fields is derived. In Sec. VI we summarize our results and our conclusions. Finally, in Appendix A we apply the adiabatic theory to calculate detachment probabilities for LP and CP fields. Throughout this paper we use the dipole approximation (which is adequate for strong field processes in moderately intense infrared laser fields) and atomic units ($\hbar = m_e = e = 1$).

## II. OVERVIEW OF THEORETICAL METHODS FOR STRONG FIELD PROCESSES

There are few efficient theoretical methods able to treat laser-atom interactions on a fully nonperturbative basis, which is necessary for describing such highly nonlinear phenomena as ATI and HHG. These methods include the numerical solution of the time-dependent Schrödinger equation (TDSE); exactly solvable models such as the quasistationary quasienergy states approach (QQES) for the zero-range potential [28]; the adiabatic approximation [29–31]; the $S$-matrix approach [32–35]; the Keldysh theory [18, 36, 37] or, equivalently, the strong field approximation [38, 39]; and the simple man (classical) model (SMM) [40]. Although exact, the TDSE approach presents two difficulties: it is highly demanding of computational resources, particularly for fields having long wavelengths or polarizations other than linear, and it provides little insight into the physics of a problem without extensive, time-consuming additional calculations to explore the relevant parameter space. The QQES method combined with the effective range theory provides a model-independent almost exact description of ATI and HHG for weakly-bound systems such as negative ions [41]. The generalization of its results to the case of atoms has been achieved heuristically (see, e.g., Refs. [42–46]) in the tunneling limit, $\gamma \to 0$, where $\gamma$ is the adiabaticity parameter introduced by Keldysh [18] [see Eq. (6) below]. The SFA is rather efficient for providing a qualitative description of the basic features of both ATI and HHG spectra. For systems bound by short-range forces it is quantitatively accurate and consistent with the QQES approach (for discussions comparing the two approaches, see Refs. [14, 41]). Finally, the SMM has provided invaluable insight into the physics of recollision processes, including HHG, but its purely classical essence is insufficient for calculating quantum mechanical ATI and HHG probabilities and interference effects.

Owing to its efficiency and qualitative accuracy, different extensions of the SFA have been developed since the early days of strong field physics, especially during the past decade, aimed at improving its quantitative accuracy for atoms, ions, and molecules. Incorporation of the Coulomb interaction into the SFA is based on the so-called perturbation theory for the action, suggested in the context of the ionization problem by Perelomov and Popov [19]. The idea stems from the fact that, within the SFA, the photoelectron motion in the continuum is described by the Volkov function – an exact solution to the Schrödinger equation for an electron in the field of a plane electromagnetic wave [47–50]. The phase of the Volkov function coincides with the classical action for an electron moving in a laser field. After ionization the photoelectron departs from the nucleus quickly, so that for most of its trajectory the laser force dominates the Coulomb one. Thus, the Coulomb interaction can be taken into account as a correction to the action due to the Coulomb energy along the photoelectron trajectory in the laser field. Owing to the quantum nature of strong field ionization from ground states of atoms, such photoelectron trajectories cannot be entirely classical: they remain Newtonian but in complex time and space. That scheme was adopted for the semiclassical representation of the SFA (both with and without the Coulomb field included) and realized via the imaginary time method (ITM) [51]. In a strong laser field, the Coulomb action calculated along such "classical" complex space-time trajectories is complex-valued and therefore changes both the absolute value and the phase of the ionization amplitude. Although small compared to the laser-induced action, it is usually numerically large and causes pronounced effects in photoelectron spectra. The trajectory-based calculation of Coulomb corrections, extended to arbitrary values of photoelectron momenta and of the Keldysh parameter, is known in the literature as the CCSFA [14, 17]. Suggested at the same time with the CCSFA and based on similar ideas, although technically different in realization, the eikonal-Volkov approximation (EVA) [52] and the analytic R-matrix theory (ARM) [53] are also used to describe Coulomb effects in ATI spectra. Applying the CCSFA, EVA, and ARM methods, several Coulomb-induced effects have been analyzed. These include the Coulomb-induced asymmetry of the photoelectron distributions produced by elliptically-polarized fields [54], the total photoionization rate at arbitrary laser frequencies [55], the low-energy structures [56], the photoelectron holographic side lobes [6], and the attoclock experiment [57] (see the review [14] for details). Recently, the ARM method has been advanced to probe Coulomb effects in HHG spectra [58].

In the general case of arbitrary photoelectron momentum and Keldysh parameter, the application of the CCSFA meets serious computational difficulties. The Coulomb correction to the action along a complex-valued laser-driven trajectory requires numerical evaluation, except in special cases. This involves in turn a topological analysis of the Coulomb potential energy as a function of complex time. Recent studies [7, 59, 60] have demonstrated that this function is not analytic over the entire complex plane but has poles and branch points that make the construction of an integration contour a complicated numerical task. One way to avoid these difficulties is to simplify the theory by replacing complex-valued trajectories by real ones [56, 61] or by reformulating the theory in such a way that complex trajectories do not appear from the very beginning [62]. Such simplifications, although efficient, obviously omit effects of "subbarrier" motion. Meanwhile the subbarrier contribution to the phase, which determines the interference structure of photoelectron distributions, was shown to be significant [63].

Yet another possibility to simplify the theory analytically without disregarding complex-time effects consists in considering its adiabatic limit, in which case a regular expansion of all relevant quantities in powers of $\gamma$ considerably facilitates calculations and provides sufficient

accuracy despite retention of only a few terms. Taking into account that the domain of strong-field ionization experiments has been recently extended to mid-infrared fields with wavelengths $\lambda \simeq 2-10\mu$m, this limit has more than academic interest. In fact, for ground states of atoms, the true tunneling regime of ionization is only accessible at mid-infrared wavelengths.

## III. DETACHMENT AMPLITUDE IN THE ADIABATIC LIMIT

Within the SFA, the strong field detachment amplitude of a weakly-bound electron can be presented in the well-known form [14, 18, 36–39] (see also Ref. [46]):

$$\mathcal{A}(\boldsymbol{p}) = \frac{1}{2\pi}\int_{-\infty}^{\infty} f_l(\boldsymbol{p},t)e^{iS(\boldsymbol{p},t)}dt, \tag{1}$$

$$S(\boldsymbol{p},t) = \int_{-\infty}^{t}\left\{\frac{1}{2}\left[\boldsymbol{p}+\boldsymbol{A}(t')\right]^2 + I_p\right\}dt', \tag{2}$$

where $\boldsymbol{p}$ is the photoelectron momentum at the detector, $\boldsymbol{A}(t)$ is the vector potential of the laser field, $I_p$ is the ionization potential, and $f_l(\boldsymbol{p},t)$ is a smooth preexponential function, whose explicit form depends on the spatial symmetry of the initial electron bound state ($l$ is the orbital momentum of the bound state). Since our analysis is focused on the exponential phase (2), this explicit form is not important. For low frequencies, we estimate the integral in (1) by the saddle point method:

$$\mathcal{A}(\boldsymbol{p}) = \sum_{\nu} a_\nu(\boldsymbol{p}), \tag{3}$$

$$a_\nu(\boldsymbol{p}) = \frac{f_l(\boldsymbol{p},t_\nu)e^{iS(\boldsymbol{p},t_\nu)}}{\sqrt{2\pi i\left(\boldsymbol{V}(t_\nu)\cdot\boldsymbol{F}(t_\nu)\right)}}, \tag{4}$$

where $\boldsymbol{V}(t) = \boldsymbol{p}+\boldsymbol{A}(t)$ is the time-dependent photoelectron velocity, $\boldsymbol{F}(t) = -\partial\boldsymbol{A}(t)/\partial t$ is the laser field strength, and the index $\nu$ numbers the saddle points, which satisfy the equation:

$$\left[\boldsymbol{p}+\boldsymbol{A}(t_\nu)\right]^2 + 2I_p = 0. \tag{5}$$

Solutions of Eq. (5) are obviously complex, $t_\nu(\boldsymbol{p}) \equiv t_\nu = \overline{t}_\nu + i\Delta_\nu$, where $\overline{t}_\nu$ and $\Delta_\nu$ are real. Only the roots $t_\nu$ with $\Delta_\nu > 0$ should be included in the sum (3), since the transition to the continuum state starts from a bound state with negative energy $-I_p$ [64].

We assume the Keldysh parameter $\gamma$ [18], defined by

$$\gamma = \frac{\kappa\omega}{F}\ , \qquad \kappa = \sqrt{2I_p} \tag{6}$$

is small, i.e., $\gamma \ll 1$, which defines the so-called adiabatic or tunneling regime of ionization. In this limit, $\omega\Delta_\nu \ll 1$ [37, 65] (see also Refs. [29–31]), and we can expand Eq. (5) as a series in the adiabatic parameter $\Delta_\nu$. Keeping terms up to second order, we obtain:

$$\boldsymbol{V}_\nu^2 - 2i\Delta_\nu\boldsymbol{V}_\nu\cdot\boldsymbol{F}_\nu - \Delta_\nu^2\left(\boldsymbol{F}_\nu^2 - \boldsymbol{V}_\nu\cdot\dot{\boldsymbol{F}}_\nu\right) + \kappa^2 = 0, \tag{7}$$

where $\boldsymbol{V}_\nu \equiv \boldsymbol{V}(\overline{t}_\nu)$, $\boldsymbol{F}_\nu \equiv \boldsymbol{F}(\overline{t}_\nu)$, and $\dot{\boldsymbol{F}}_\nu \equiv \partial\boldsymbol{F}(t)/\partial t|_{t=\overline{t}_\nu}$. Separating the real and imaginary parts of Eq. (7), we obtain an equation for $\overline{t}_\nu$:

$$\boldsymbol{V}_\nu\cdot\boldsymbol{F}_\nu = 0, \tag{8}$$

and an expression for $\Delta_\nu$:

$$\Delta_\nu = \frac{\varkappa_\nu}{\mathcal{F}_\nu}, \tag{9}$$

where

$$\varkappa_\nu = \sqrt{\kappa^2 + \boldsymbol{V}_\nu^2}, \tag{10a}$$

$$\mathcal{F}_\nu = \sqrt{\boldsymbol{F}_\nu^2 - \boldsymbol{V}_\nu\cdot\dot{\boldsymbol{F}}_\nu}. \tag{10b}$$

Equation (8) implies that the first time-derivative of the electron's kinetic energy in the laser field is zero [65]. Since $\boldsymbol{F}_\nu^2 - \boldsymbol{V}_\nu\cdot\dot{\boldsymbol{F}}_\nu > 0$ ($\Delta_\nu$ is real), at the moment $t = \overline{t}_\nu$ both the electron kinetic energy and $\varkappa_\nu$ are minimized. Expanding Eq. (2) as a series in $\Delta_\nu$ and keeping terms up to third order, we obtain:

$$S(\boldsymbol{p},t_\nu) \approx S(\boldsymbol{p},\overline{t}_\nu) + i\frac{\varkappa_\nu^3}{3\mathcal{F}_\nu}. \tag{11}$$

The scalar product $\boldsymbol{V}(t_\nu)\cdot\boldsymbol{F}(t_\nu)$ in Eq. (4) also can be simplified: expanding it up to first order in $\Delta_\nu$ and taking into account Eq. (8), we obtain:

$$\boldsymbol{V}(t_\nu)\cdot\boldsymbol{F}(t_\nu) \approx -i\Delta_\nu\mathcal{F}_\nu^2. \tag{12}$$

Collecting Eqs. (9), (11), and (12), we obtain for the partial detachment amplitude in the adiabatic limit:

$$a_\nu(\boldsymbol{p}) = \frac{f_l(\boldsymbol{p},\overline{t}_\nu)e^{iS(\boldsymbol{p},\overline{t}_\nu)}}{\sqrt{2\pi\varkappa_\nu\mathcal{F}_\nu}}e^{-\varkappa_\nu^3/(3\mathcal{F}_\nu)}. \tag{13}$$

This result is valid for $\omega\Delta_\nu \ll 1$, which requires, in addition to being in the tunneling regime, that the electron kinetic energy at the time of release is small, $\boldsymbol{V}_\nu^2 \ll p_F^2$, where $p_F = F/\omega$ is the characteristic electron quiver momentum in the laser field (i.e., its field momentum). The latter follows from the estimate

$$\omega^2\Delta_\nu^2 \sim \gamma^2 + \boldsymbol{V}_\nu^2/p_F^2\ . \tag{14}$$

In practice, $\boldsymbol{V}_\nu^2$ should not exceed by much the value $\kappa^2$.

Consider now two simple and simultaneously common cases of monochromatic LP and CP fields. For the LP field, $\boldsymbol{F}(t) = \boldsymbol{e}_z F\cos\omega t$, so that Eq. (8) becomes

$$p_z - p_F\sin\omega\overline{t}_\nu = 0, \tag{15}$$

where $p_z = (\boldsymbol{p}\cdot\boldsymbol{e}_z)$, and may be solved analytically:

$$\omega\overline{t}_\nu^{(+)} = \arcsin\frac{p_z}{p_F} + 2\pi\nu, \tag{16a}$$

$$\omega\overline{t}_\nu^{(-)} = \pi - \arcsin\frac{p_z}{p_F} + 2\pi\nu\ . \tag{16b}$$

In this case, for any $\nu$:

$$\boldsymbol{V}_{\rm lin}^2 = \boldsymbol{V}_\nu^2 = p_\perp^2 = p^2 - p_z^2, \tag{17a}$$

$$\varkappa_{\rm lin} = \varkappa_\nu = \kappa\sqrt{1+\left(p_\perp/\kappa\right)^2}, \tag{17b}$$

$$\mathcal{F}_{\rm lin} = \mathcal{F}_\nu = F\sqrt{1-\left(p_z/p_F\right)^2}, \tag{17c}$$

$$\omega\Delta_{\rm lin} = \omega\Delta_\nu = \gamma\sqrt{\frac{1+\left(p_\perp/\kappa\right)^2}{1-\left(p_z/p_F\right)^2}}. \tag{17d}$$

Explicit forms of $\mathcal{F}_\nu$ and $\Delta_\nu$ show that the momentum distribution of photoelectrons determined by $|a_\nu(\boldsymbol{p})|^2$, takes its maximum value at $p_\perp = 0$ and $p_z = 0$ [see Eqs. (A5), (17b), and (17c)]. For $p_\perp \ll \kappa$, $p_z \ll p_F$, expansion of Eqs. (17b) and (17c) respectively in powers of $\left(p_z/p_F\right)^2$ and $\left(p_\perp/\kappa\right)^2$ shows that it has a Gaussian shape, in agreement with previous studies [12, 37, 66].

For a CP field, $\boldsymbol{F}(t) = F\{\cos\omega t; \sin\omega t\}$, the equation for $\bar{t}_\nu$ simplifies since $\boldsymbol{F}(t)\cdot\boldsymbol{A}(t) = 0$:

$$\boldsymbol{p}\cdot\boldsymbol{F}_\nu = p_{||}F\cos(\omega\bar{t}_\nu - \varphi) = 0, \tag{18}$$

where $\varphi$ is the angle between the $X$-axis and the photoelectron momentum projection $\boldsymbol{p}_{||}$ on the polarization plane. The desired solution of Eq. (18) is

$$\omega\bar{t}_\nu = \frac{\pi}{2} + \varphi + 2\pi\nu, \tag{19}$$

and leads to the following result:

$$\boldsymbol{V}_\nu^2 = \left(p_{||} - p_F\right)^2 + p_\perp^2, \quad \mathcal{F}_\nu = F\sqrt{p_{||}/p_F}, \tag{20a}$$

$$\omega\Delta_\nu = \sqrt{\frac{\gamma^2 + \left(1 - p_{||}/p_F\right)^2 + \left(p_\perp/p_F\right)^2}{p_{||}/p_F}}, \tag{20b}$$

$$\varkappa_\nu = \sqrt{\kappa^2 + p_\perp^2 + \left(p_{||} - p_F\right)^2}\ , \tag{20c}$$

where $p_\perp^2 = p^2 - p_{||}^2$. In contrast to the LP field case, the partial amplitude $a_\nu(\boldsymbol{p})$ for the CP field has its maximum at $p_{||} = p_F$, $p_\perp = 0$ [see Eqs. (A9) and (A10)] in agreement with Refs. [36, 37]. Near $p_{||} = p_F$ the distribution is Gaussian and axially symmetric about the laser field propagation direction. These formulas apply if $p_\perp$ and $p_{||}$ do not deviate from $p_{||} = p_F$, $p_\perp = 0$ by more than several $\kappa$. Further analysis and applications of the adiabatic approximation for LP and CP fields are given in Appendix A.

## IV. COULOMB CORRECTIONS FOR PHOTOELECTRON MOMENTUM DISTRIBUTIONS IN THE ADIABATIC REGIME

The phase $S(\boldsymbol{p}, t_\nu)$ in Eq. (4) is the classical action for an electron moving in the time-dependent field $\boldsymbol{F}(t)$ along a trajectory satisfying Newton's equation and specified by the boundary conditions:

$$\left(\frac{d\boldsymbol{r}(t)}{dt}\right)^2\Bigg|_{t=t_\nu} = -\kappa^2, \quad \boldsymbol{r}(t_\nu) = \boldsymbol{0}. \tag{21}$$

The Coulomb interaction can be taken into account by calculating a correction to the Coulomb-free action in Eq. (4) along the Coulomb-free trajectory specified by conditions (21) [19]. Detailed descriptions of this method are given in recent reviews [12, 14, 15]. Here we sketch briefly the algorithm, which has both analytical and topological parts.

The analytic part includes the following five steps:
**(i)** Find the Coulomb-free electron trajectories, $\boldsymbol{r}(t)$, in the laser field, $\boldsymbol{F}(t)$, satisfying (21).
**(ii)** Find the points $t^{(\rm bp)}$ (different from $t_\nu$) in the complex time plane at which $\boldsymbol{r}^2(t^{(\rm bp)}) = 0$. These complex times are branch points of the function $\sqrt{\boldsymbol{r}^2(t)}$.
**(iii)** Calculate the Coulomb action along the Coulomb-free electron trajectory $\boldsymbol{r}(t)$:

$$\delta S(\zeta) = \int_{\mathcal{C}} \frac{Z}{\sqrt{\boldsymbol{r}^2(t)}}dt, \tag{22}$$

where $Z$ is the residual atomic charge ($Z = 0$ and 1 for negative ions and neutral atoms, respectively). The semi-infinite integration contour $\mathcal{C}$ connecting the start time ($t_\nu$) and the detection time ($t \to \infty$) is chosen in such a way that it avoids cuts generated by the branch points $t^{(\rm bp)}$. The integral (22) is logarithmically divergent at the saddle point, so that the integration must start from a complex time $t = \zeta$ close to $t_\nu$. The value of $\zeta$ will be eliminated from the final result through a regularization procedure (see the next step).
**(iv)** Regularize $\delta S$ by matching it to the field-free Coulomb action at $\zeta = t_\nu$:

$$\Delta S_\nu(\boldsymbol{p}) = \lim_{\zeta\to t_\nu}\left(\delta S(\zeta) + i\frac{Z}{\kappa}\ln|\kappa^2(\zeta - t_\nu)|\right); \tag{23}$$

**(v)** Calculate the Coulomb factor in the ionization amplitude, $\exp(i\Delta S_\nu)$. If the Coulomb correction is a purely imaginary quantity that is the same for all $\nu$ (as in the case of monochromatic fields), it gives a momentum-dependent Coulomb factor in the ionization amplitude:

$$Q_\nu(\boldsymbol{p}) = e^{-{\rm Im}\Delta S_\nu(\boldsymbol{p})}.$$

The topological part of the problem concerns the geometry of the integration contour $\mathcal{C}$. In general this is a complicated computational problem, since it requires the mapping of all branch points and poles of the function $1/\sqrt{\boldsymbol{r}^2(t)}$ in order to develop a contour that lies on a single sheet of the Riemann surface. Examples of this kind of topological analysis can be found in Refs. [7, 60]. Except for the saddle point $t_\nu$, which generates a first-order pole of the Coulomb potential energy [whose divergent contribution is safely eliminated by the matching procedure (23)], most of the zeros of the function $\boldsymbol{r}^2(t)$ can be associated with close approaches of the photoelectron to the parent ion due to its oscillations in a time-dependent laser field. As shown in Ref. [7], the contributions of these complex-time returns to the action (23) can be significant, with a correspondingly large

effect on the photoelectron spectrum if the parameter $\gamma Z/\kappa > 1$ (see examples in Ref. [7]). In the adiabatic limit that we consider, however, this value is small (owing to $Z = 1$, $\kappa \simeq 1$), so that the branch points associated with such returns do not play a significant role. Physically, it can be justified by the increased spreading of the photoelectron wave packet with increasing laser period so that the electrons drift away from the lateral direction (for a LP field), and hence close approaches become less and less likely. Thus we disregard the branch points generated by returns. Consequently, only one pair of branch points remains (see below), thus allowing for a fully analytic treatment.

For $\omega\Delta_\nu \ll 1$, a trajectory in the integral (22) can be calculated by restricting the time $|t - t_\nu|$ to a small fraction of the laser period and expanding in $\tau \equiv t - \overline{t}_\nu$ :

$$\frac{d\boldsymbol{r}(t)}{dt} = \boldsymbol{p} + \boldsymbol{A}(t) \approx \boldsymbol{V}_\nu - \boldsymbol{F}_\nu\tau - \dot{\boldsymbol{F}}_\nu\frac{\tau^2}{2}. \qquad (24)$$

Integrating Eq. (24) over $\tau$ and satisfying the initial condition at $\tau = i\Delta_\nu$ gives the trajectory:

$$\boldsymbol{r}(t) = \boldsymbol{V}_\nu(\tau - i\Delta_\nu) - \frac{\boldsymbol{F}_\nu}{2}\left(\tau^2 + \Delta_\nu^2\right) - \frac{\dot{\boldsymbol{F}}_\nu}{6}(\tau^3 + i\Delta_\nu^3). \quad (25)$$

For convenience, we introduce a new variable $\xi$, $\tau = i\xi$, so that $\boldsymbol{r}_c(\xi) \equiv \boldsymbol{r}(\overline{t}_\nu + i\xi)$ takes the form:

$$\boldsymbol{r}_c(\xi) = i\boldsymbol{V}_\nu(\xi - \Delta_\nu) + \frac{\boldsymbol{F}_\nu}{2}(\xi^2 - \Delta_\nu^2) + i\frac{\dot{\boldsymbol{F}}_\nu}{6}(\xi^3 - \Delta_\nu^3). \quad (26)$$

Using Eqs. (8)-(10) and (26), $\boldsymbol{r}_c^2(\xi)$ including terms up to $(\xi - \Delta_\nu)^4$ can be presented as:

$$\boldsymbol{r}_c^2(\xi) = (\xi - \Delta_\nu)^2\left[\kappa^2 + (\xi - \Delta_\nu)\Delta_\nu\mathcal{F}_\nu^2 + \frac{(\xi - \Delta_\nu)^2}{4}\left(\mathcal{F}_\nu^2 - \frac{\boldsymbol{V}_\nu \cdot \dot{\boldsymbol{F}}_\nu}{3}\right)\right], \qquad (27)$$

in which all terms in $\Delta_\nu$ (as well as those involving $\omega\Delta_\nu$) have been dropped if they do not determine a leading term. Equation (27) explicitly shows that $\boldsymbol{r}_c^2(\xi)$ behaves quadratically at $\xi \to \Delta_\nu$:

$$\boldsymbol{r}_c^2(\xi) \approx \kappa^2(\xi - \Delta_\nu)^2, \qquad (28)$$

and the integral (22) diverges logarithmically at $\zeta \to t_\nu$ [19]. Moreover, the function in the square bracket of Eq. (27) becomes zero at $\xi = \xi_\pm^{(\mathrm{bp})}$:

$$\xi_{\pm,\nu}^{(\mathrm{bp})} = -\Delta_\nu\frac{\mathcal{F}_\nu^2 + \boldsymbol{V}_\nu \cdot \dot{\boldsymbol{F}}_\nu/3}{\mathcal{F}_\nu^2 - \boldsymbol{V}_\nu \cdot \dot{\boldsymbol{F}}_\nu/3} \pm 2\frac{\sqrt{\boldsymbol{V}_\nu^2\mathcal{F}_\nu^2 + \kappa^2\boldsymbol{V}_\nu \cdot \dot{\boldsymbol{F}}_\nu/3}}{\mathcal{F}_\nu^2 - \boldsymbol{V}_\nu \cdot \dot{\boldsymbol{F}}_\nu/3}. \qquad (29)$$

Using Eq. (10b), the denominators in Eq. (29) become

$$\mathcal{F}_\nu^2 - \frac{\boldsymbol{V}_\nu \cdot \dot{\boldsymbol{F}}_\nu}{3} = \frac{4}{3}\left(\mathcal{F}_\nu^2 - \frac{\boldsymbol{F}_\nu^2}{4}\right).$$

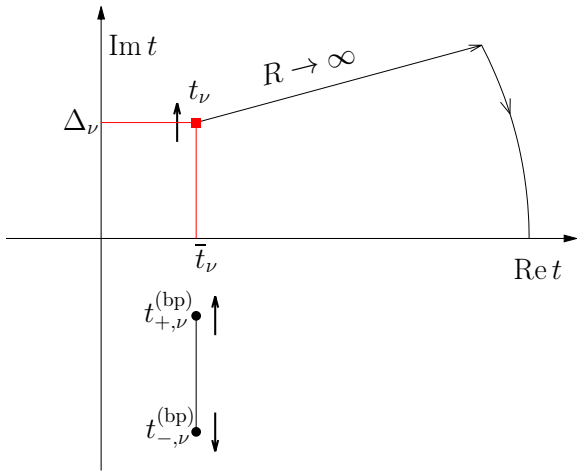


FIG. 1. Map of the saddle ($t_\nu$) and branch points ($t_{\pm,\nu}^{(\mathrm{bp})}$) in the complex plane of time $t$. The vertical segment with endpoints $t_{\pm,\nu}^{(\mathrm{bp})}$ is a cut in the Riemann surface. Arrows show the directions in which the saddle and the branch points move with increasing $\boldsymbol{V}_\nu$. The arc shown by a thin solid line represents a possible integration path.

Under the condition $\omega\Delta_\nu \ll 1$, $\xi_{\pm,\nu}^{(\mathrm{bp})}$ is real and thus two branch points, $t_{\pm,\nu}^{(\mathrm{bp})} = \overline{t}_\nu + i\xi_{\pm,\nu}^{(\mathrm{bp})}$, for given $\nu$ are placed on the line $\mathrm{Re}\, t = \overline{t}_\nu$. With increasing $\boldsymbol{V}_\nu$ they move along this line in positive (for the "+" solution) and negative (for the "−" solution) directions (see Fig. 1). Thus, in order to make $1/\sqrt{\boldsymbol{r}^2(t)}$ a bijective function, we cut the complex plane by a segment bounded by the points $t_{\pm,\nu}^{(\mathrm{bp})}$ (see Fig. 1). Since $1/\sqrt{\boldsymbol{r}^2(t)} \propto 1/t$ for large $t$, we can choose any integration path that avoids the cut, starts near the point $t_\nu$, and ends at any remote point on the real time axis. For example, the integration path shown in Fig. 1 consists of a straight semi-infinite line starting from $\zeta \approx t_\nu$ and an arc of infinitely large radius. Evidently, this topology of cuts, branch, and saddle points holds only in the case $\mathcal{F}_\nu^2 > \boldsymbol{F}_\nu^2/4$ and assumes the validity of the cubic approximation for $\boldsymbol{r}(t)$ [cf. Eq. (26)].

In the case $\mathcal{F}_\nu^2 < \boldsymbol{F}_\nu^2/4$, $t_{-,\nu}^{(\mathrm{bp})}$ is above the saddle point $t_\nu$, while $t_{+,\nu}^{(\mathrm{bp})}$ is located below $t_\nu$. In the special case $\mathcal{F}_\nu^2 = \boldsymbol{F}_\nu^2/4$, one branch point ($t_{-,\nu}^{(\mathrm{bp})}$) is at infinity, while $t_{+,\nu}^{(\mathrm{bp})}$ is located just below the saddle point $t_\nu$ in the first quadrant of the complex plane. With *decreasing* $\boldsymbol{V}_\nu$, the branch points move toward each other along the vertical line $t = \overline{t}_\nu$, so that cuts can be drawn as vertical lines from points $t_{-,\nu}^{(\mathrm{bp})}$ (straight up) and $t_{+,\nu}^{(\mathrm{bp})}$ (straight down). Note that this case is interesting only from a mathematical point of view, since it is realized only for $\omega\Delta_\nu > 1$, so that the adiabatic approximation is inapplicable.

Substituting Eq. (27) into Eq. (22) and using Eq. (23), we analytically calculate the integral (22) (see Ref. [67])

and obtain in the limit $\zeta \to t_\nu$:

$$\Delta S_\nu = -i\frac{Z}{\kappa}\ln\left|\frac{4\kappa^3}{\mathcal{F}_\nu\left[\sqrt{1+\frac{\boldsymbol{V}_\nu^2}{\kappa^2}}+\frac{2}{\sqrt{3}}\sqrt{1-\frac{\boldsymbol{F}_\nu^2}{4\mathcal{F}_\nu^2}}\right]}\right|. \quad (30)$$

Then we obtain the Coulomb factor $Q_\nu$ [=exp($i\Delta S_\nu$)],

$$Q_\nu = Q_{\rm stat}^{(\nu)}\mathcal{R}^{(\nu)}, \quad (31)$$

where

$$Q_{\rm stat}^{(\nu)} = \left(\frac{2\kappa^3}{F_\nu}\right)^{Z/\kappa}, \quad F_\nu = \sqrt{\boldsymbol{F}_\nu^2}, \quad (32)$$

$$\mathcal{R}^{(\nu)} = \left(\frac{2F_\nu}{\mathcal{F}_\nu\left[\sqrt{1+\frac{\boldsymbol{V}_\nu^2}{\kappa^2}}+\frac{2}{\sqrt{3}}\sqrt{1-\frac{\boldsymbol{F}_\nu^2}{4\mathcal{F}_\nu^2}}\right]}\right)^{Z/\kappa}. \quad (33)$$

The Coulomb correction factors in Eqs. (31)–(33) are the main results of this work. In order to obtain the Coulomb-corrected ionization amplitude, $\tilde{\mathcal{A}}(\boldsymbol{p})$, each partial amplitude $a_\nu(\boldsymbol{p})$ in the sum in Eq. (3) must be multiplied by the factor $Q_\nu$:

$$\tilde{\mathcal{A}}(\boldsymbol{p}) = \sum_\nu Q_\nu a_\nu(\boldsymbol{p}), \quad (34)$$

where $a_\nu$ is given by Eq. (13). In the limit $\boldsymbol{V}_\nu \to 0$, $\mathcal{R}^{(\nu)} \to 1$ and $Q_{\rm stat}^{(\nu)}$ in (31) is the well-known static field Coulomb factor [20, 37], but taken for the field amplitude at the instant of ionization. Note that the adiabatic result (30) for the Coulomb correction is purely imaginary.

In order to obtain Coulomb factors for LP and CP fields from the general result (33), we need an explicit expression for the scalar product $\boldsymbol{V}_\nu \cdot \dot{\boldsymbol{F}}_\nu$. From Eqs. (16) and (19) it follows that for a LP field:

$$\boldsymbol{V}_\nu \cdot \dot{\boldsymbol{F}}_\nu = 0, \quad (35)$$

and for a CP field

$$\boldsymbol{V}_\nu \cdot \dot{\boldsymbol{F}}_\nu = F^2\left(1-\frac{p_{||}}{p_F}\right). \quad (36)$$

Using Eqs. (17), (33), (35), and the fact that for a LP field $\boldsymbol{V}_\nu^2 = p_\perp^2$ and $F_\nu^2 = \mathcal{F}_\nu^2$, we obtain for a LP field:

$$\mathcal{R} = \left(\frac{2}{1+\sqrt{1+(p_\perp/\kappa)^2}}\right)^{Z/\kappa}, \quad (37)$$

where we have dropped the index $\nu$ as unnecessary. For $p_\perp \ll \kappa$, $\mathcal{R}$ can be expanded in a series in $p_\perp/\kappa$:

$$\mathcal{R} \approx 1 - \frac{Zp_\perp^2}{4\kappa^3} + \frac{Zp_\perp^4}{32\kappa^5}\left(3+\frac{Z}{\kappa}\right). \quad (38)$$

Since for a LP field $\boldsymbol{V}_\nu$ has zero projection on the polarization axis [see Eq. (29)], $\xi_{\pm,\nu}^{(\rm bp)} < 0$, and the integration contour can be handled in a standard way: vertically down to the real axis, and then along it [59]. The static factor $Q_{\rm stat}$ has a singularity for $p_z = p_F$:

$$Q_{\rm stat}^{(\rm lin)} = \left(\frac{2\kappa^3}{F\sqrt{1-(p_z/p_F)^2}}\right)^{Z/\kappa}. \quad (39)$$

This singularity shows the limitation of the adiabatic approximation for finding saddle points. Indeed, for $p_z > p_F$ Eq. (15) cannot be solved for real times and a more accurate equation for finding the saddle points should be used. For $p_z \to p_F$, $\mathcal{F}_\nu$ tends to zero [see Eq. (17c)] and the adiabatic approximation breaks down [since, according to Eq. (17d), $\omega\Delta_\nu \to \infty$]. In Fig. 2(a) we show the dependence of $\omega\Delta_\nu$ on $p_z$ for three values of $p_\perp$, while in Fig. 2(b) we show the dependence of $Q_{\rm stat}^{(\rm lin)}$ on $p_z$. As $p_z$ increases, both $\omega\Delta_\nu$ and $Q_{\rm stat}^{(\rm lin)}$ gradually increase. For a LP field, the factor $Q_{\rm stat}^{(\rm lin)}$ does not depend on $p_\perp$, while the accuracy of the adiabatic Coulomb correction decreases with increasing $p_\perp$, owing to the increase in the parameter $\omega\Delta_\nu$. Since the factor $\mathcal{R}$ decreases with increasing $p_\perp$ [and does not depend on $p_z$, see Fig. 2(c)], the Coulomb factor decreases with increasing $p_\perp$.

For a CP field, using (20a), the factor $\mathcal{R}$ has the form:

$$\mathcal{R} = \left(\frac{2\gamma}{\omega\Delta_\nu\frac{p_{||}}{p_F}+\gamma\sqrt{\frac{4p_{||}}{3p_F}-\frac{1}{3}}}\right)^{Z/\kappa}, \quad (40)$$

where $\omega\Delta_\nu$ is given by Eq. (20b). It is worthwhile to note that the result (40) for $p_{||} = p_F$ coincides with $\mathcal{R}$ for a LP field in Eq. (37). In contrast to the case of LP field, $Q_{\rm stat}$ for a CP field does not depend on the momentum, since $\boldsymbol{F}_\nu^2 = F^2$. However, the factor $\mathcal{R}$ has a branch point singularity at $p_{||} = p_F/4$. For $p_{||} \le p_F/4$, $\omega\Delta_\nu$ takes values greater than unity and the adiabatic approximation, as well as the results in this approximation, are invalid and require special consideration. Furthermore, for such values of $p_{||}$ the probability of ionization is exponentially small. In Fig. 3 we present the dependence of $\omega\Delta_\nu$ and $\mathcal{R}$ on $p_{||}$ for three values of $p_\perp$. Neither dependence is symmetric with respect to the momentum $p_{||} = p_F$. Moreover, the minimum in the dependence of $\omega\Delta_\nu$ on $p_{||}$ for fixed $p_\perp$ is shifted toward higher momenta with respect to $p_{||} = p_F$ and also moves to the right with increasing $p_\perp$ [see Fig. 3(a)].

The Coulomb-induced modifications of ATI spectra become most apparent for longitudinal electron emission in a LP field. In this case, the squared factor (39) increases as $(1-p_z^2/p_F^2)^{-Z/\kappa}$, thus slightly reducing the (negative) slope of the spectrum. In the lateral direction, the slope of the spectrum instead becomes more negative (37), but,

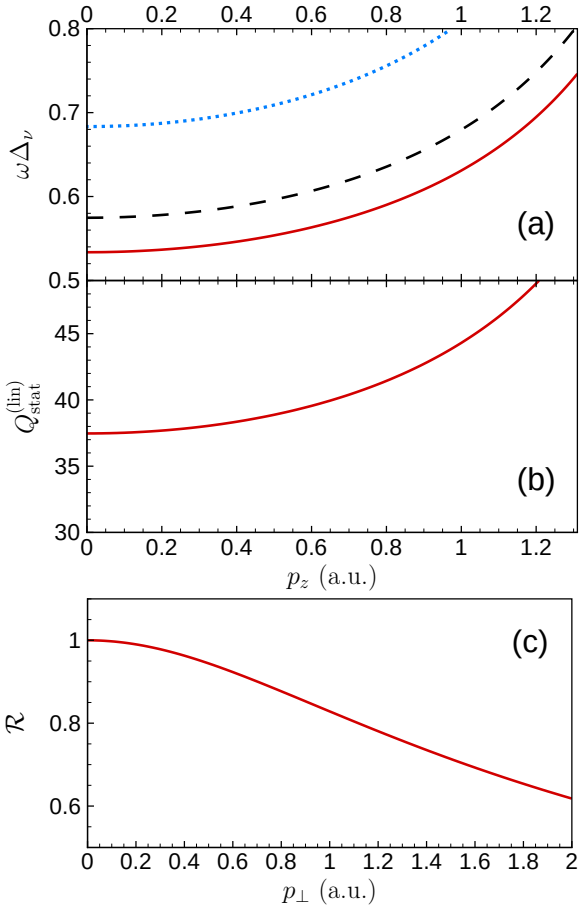


FIG. 2. Momentum dependence of the adiabatic parameter and Coulomb correction factors for a monochromatic LP field. (a) Dependence of $\omega\Delta_\nu$ on $p_z$ for three values of $p_\perp$ [see Eq. (17d)]: Solid (red) line: $p_\perp = 0$; dashed (black) line: $p_\perp = 0.4\kappa$; dotted (blue) line: $p_\perp = 0.8\kappa$. (b) Dependence of $Q_{\rm stat}^{\rm (lin)}$ on $p_z$ [see Eq. (39)]. (c) Dependence of $\mathcal{R}$ on $p_\perp$ [see Eq. (37)]. Calculations employed a field intensity $I = 10^{14}$W/cm$^2$, $\lambda = 1.6$ $\mu$m, $Z = 1$, $\kappa = 1$ a.u., and $\gamma = 0.53$.

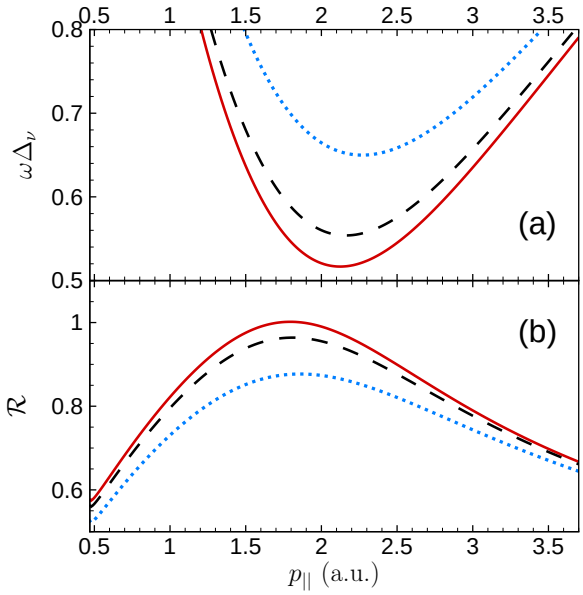


FIG. 3. Dependence of (a) the adiabatic parameter $\omega\Delta_\nu$ (20b) and (b) the Coulomb correction factor $\mathcal{R}$ (40) on $p_{||}$ for a monochromatic CP field and three values of $p_\perp$: Solid (red) lines: $p_\perp = 0$; dashed (black) lines: $p_\perp = 0.4\kappa$; dotted (blue) lines: $p_\perp = 0.8\kappa$. Calculations employed a field intensity $I = 10^{14}$W/cm$^2$, $\lambda = 1.6$ $\mu$m, $Z = 1$, $\kappa = 1$ a.u., $\gamma = 0.53$, $p_F = 1.87$ a.u., and $Q_{\rm stat}^{\rm (circ)} = 37.47$.

as the lateral distribution decreases much faster than the longitudinal one, the lateral Coulomb effect is expected to be less noticeable. In order to confirm the adiabatic Coulomb effect in photoelectron distributions along the polarization direction, in Fig. 4 we compare experimental data on tunneling ionization of Ne [72] and Ar [2] atoms to SFA predictions with and without the CC. In our theoretical calculations we used a Gaussian shape for the laser pulses and chose the peak intensities, pulse durations, and laser wavelengths appropriate for the two experiments, i.e., $10^{15}$ W/cm$^2$, 50 fs, and 795 nm for Ref. [72], and $1.5 \times 10^{14}$ W/cm$^2$, 25 fs, and 2 $\mu$m for Ref. [2]. The theoretical results in Fig. 4(a) were integrated over the lateral momentum and focally averaged, while those in Fig. 4(b) were only focal averaged for $p_\perp = 0$. Owing to the large difference in the absolute values of the theoretical results with and without the CC, the results without the CC were scaled to the results including the CC in order to match the two results at low electron energies.

Owing to focal averaging of the electron signals in Refs. [2, 72], the experimental photoelectron spectra are structureless, with no well-defined ATI peaks or interference structures. Such data are particularly useful for verifying our theoretical results, as the monotonic decrease of the electron yields [for $p_{||} > 0.4$ a.u. in Fig. 4(a) and for $p^2/2 > 0.3$ a.u. in Fig. 4(b)] allows for a high-precision comparison of the slopes of the spectra. [Note that the low-energy features in the spectra in Fig. 4, i.e., the resonant ATI peaks that survive focal averaging [72] in Fig. 4(a) and the low-energy structure (LES) [2] in Fig. 4(b), are beyond the scope of our adiabatic treatment, which ignores the bound atomic states responsible for resonant structures and the soft recollisions that lead to the emergence of the LES [56, 73].] The comparisons in Fig. 4 and Table I show that the theoretical results including our Coulomb factor significantly improve agreement with the experimental data over the electron energy range from a few eV (i.e., above the positions of the resonant ATI features and the LES) and $\sim u_p = p_F^2/4$. For higher photoelectron energies (beyond the scale of Fig. 4) approaching $2u_p$, the adiabatic approximation fails and the factor (39) begins to overestimate the ionization probability. In this part of the spectrum, non-adiabatic effects related to the first photoelectron recollision come into play and lead to a considerable modification of the Coulomb factor [7]. These nonadiabatic effects do not allow for an analytic treat-

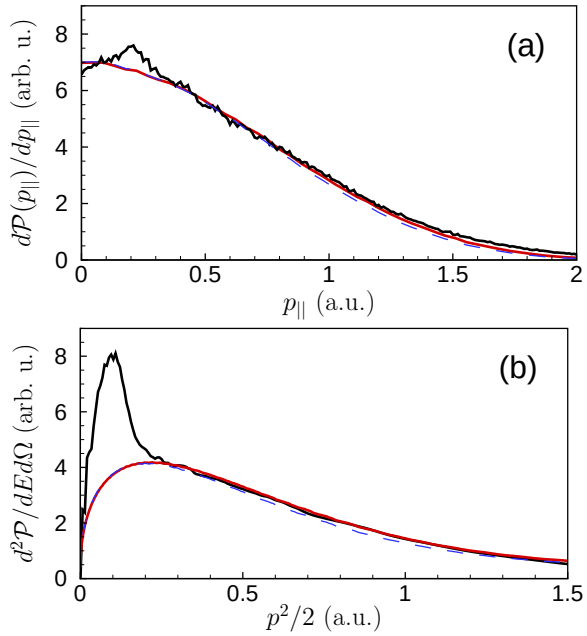


FIG. 4. Comparisons of present theoretical results with experimental photoelectron spectra. (a) Longitudinal photoelectron momentum distribution for ionization of Ne by a linearly-polarized laser field with $\lambda = 795$ nm and peak intensity $10^{15}$ W/cm$^2$. (b) Longitudinal photoelectron energy distribution for ionization of Ar by a linearly-polarized laser field with $\lambda = 2$ $\mu$m and peak intensity $1.5 \times 10^{14}$ W/cm$^2$. *Structured (black) solid lines*: experimental data, in (a) from Ref. [72] and in (b) from Ref. [2]). *Smooth (red) solid lines*: present focal-averaged results including the CC [cf. Eq. (34)]. *Dashed (blue) lines*: present focal-averaged results without the CC [cf. Eqs. (3) and (13)].

TABLE I. Comparisons of present theoretical results with experimental photoelectron spectra (arb. u.) for Ne [72] and for Ar [2] for three particular momenta in Fig. 4(a) and three particular photoelectron energies in Fig. 4(b). The theoretical SFA results with and without the CC factor correspond to the smooth solid (red) curve and the dashed (blue) curve results respectively in Fig. 4. See the caption of Fig. 4 and the text for details of the theoretical calculations.

| $p_{\|\|}$ (a.u.) | Expt. [72] | With CC | Without CC |
|---|---|---|---|
| 0.5 | 5.63 | 5.59 | 5.47 |
| 1 | 3.00 | 2.83 | 2.68 |
| 1.5 | 0.90 | 0.79 | 0.68 |
| $p^2/2$(a.u.) | Expt. [2] | With CC | Without CC |
| 0.5 | 3.22 | 3.31 | 3.13 |
| 1 | 1.43 | 1.45 | 1.28 |
| 1.5 | 0.52 | 0.64 | 0.57 |

ment.

For noble gas atoms with ionization potentials close to that of the hydrogen atom, the effective principal quantum number that determines the magnitude of the Coulomb factors derived above is $n^* = Z/\kappa \simeq 1$. As a result, the momentum-dependent adiabatic Coulomb effects shown in Figs. 2-5 remain rather modest. In contrast, for alkali atoms, which have relatively small ionization potentials, the effective principal quantum numbers are relatively large (e.g., $n^* = 1.59,\ 1.63$ and 1.87 for Li, Na and Cs respectively), which magnifies the Coulomb effect. This magnification is even larger in the case of highly-charged ions of noble gas atoms, for which $n^* \gtrsim 3$.

## V. COULOMB CORRECTIONS FOR HHG IN THE ADIABATIC REGIME

The adiabatic analysis presented above for the Coulomb correction for nonlinear laser ionization processes can also be used to analyze HHG spectra and high-energy electrons in ATI processes. The physics of both of these laser-induced processes is well described by the rescattering scenario [11, 40, 68, 69], which is based on analyzing the contributions of closed photoelectron trajectories. These trajectories start at time $t_i$ and return at time $t_f$, when the photoelectron either recombines with emission of a photon or rescatters to form the high-energy ATI plateau. The Coulomb correction for closed trajectories requires: (i) an additional regularization of an integral similar to (22) at the moment of recombination ($t_f$); and (ii) a more detailed topological analysis of the saddle and branch points. Our analysis is in progress and will be presented elsewhere. Nevertheless, it can be shown that, for a low-frequency laser field and either a high-energy photon or electron, the returning part of a closed trajectory gives a negligible contribution into the imaginary part of the Coulomb correction to the action. Indeed, the integration contour for the Coulomb correction in this case connects two points in the complex plane, $t_i$ and $t_f$, with the imaginary part of $t_f$ much smaller than that of $t_i$. Due to analyticity of the integrand in Eq. (22), we can deform the contour so that it comprises two paths: the first path (ionization) starts at the saddle point $t_i$ and goes to infinity, while the second path (return or recombination) starts from infinity and arrives at $t_f$. As noted in Sec. IV, in the adiabatic limit the major contribution to the Coulomb integral is accumulated in the vicinity of saddle points. This contribution is determined by the behavior of $\boldsymbol{r}^2(t)$ in that part of the complex time plane: for the saddle point $t_i$, $\boldsymbol{r}^2(t) \approx -\kappa^2(t-t_i)^2$ and thus the ionization path integral is given by the scaling factor $Z/(i\kappa)$ [see Eq. (30)] and is purely imaginary, while for the saddle point $t_f$, $\boldsymbol{r}^2(t) \approx \dot{\boldsymbol{r}}^2(t_f)(t-t_f)^2$ and the corresponding scaling factor is given by the Sommerfeld parameter $Z/\sqrt{\dot{\boldsymbol{r}}^2(t_f)}$, which is real and, for high energy harmonics or electrons, is of order $Z\omega/F < 1$. Thus, the contribution to the Coulomb integral from the returning path is mostly real and therefore is not expected to have a significant effect on HHG and ATI spectra. This qualitative analysis is supported by the fairly good agreement

of calculated TDSE results with analytic results [42–46], in which the Coulomb effects are accounted for heuristically in the ionization and recombination (or rescattering) steps. Below, we focus on the Coulomb correction for HHG spectra.

The real part of the complex times $t_i$, $\overline{t}_i = \mathrm{Re}\, t_i$, and $t_f$ (neglecting the imaginary part of $t_f$) satisfy the equations [70]:

$$\frac{\partial}{\partial \overline{t}_i} \boldsymbol{K}_i^2 = 0, \tag{41a}$$

$$\boldsymbol{K}_f^2 = 2E, \tag{41b}$$

where $E = \Omega - I_p$, $\Omega$ is the harmonic frequency and

$$\boldsymbol{K}_i = \boldsymbol{A}(\overline{t}_i) - \frac{1}{t_f - \overline{t}_i} \int_{\overline{t}_i}^{t_f} \boldsymbol{A}(\xi) d\xi, \tag{42}$$

$$\boldsymbol{K}_f = \boldsymbol{A}(t_f) - \frac{1}{t_f - \overline{t}_i} \int_{\overline{t}_i}^{t_f} \boldsymbol{A}(\xi) d\xi. \tag{43}$$

The saddle point $t_i$ associated with tunneling has the imaginary part, $\Delta = \mathrm{Im}\, t_i$ [70]:

$$\Delta = \frac{\sqrt{\boldsymbol{K}_i^2 + \kappa^2}}{\mathcal{F}}, \quad \mathcal{F} = \sqrt{\frac{1}{2} \frac{\partial^2 \boldsymbol{K}_i^2}{\partial \overline{t}_i^2}}, \tag{44}$$

From Eq. (41a), one finds that $\mathcal{F}$ satisfies the same equation as for ionization [cf. Eq. (10b)]:

$$\mathcal{F} = \sqrt{\boldsymbol{F}_i^2 - \boldsymbol{K}_i \cdot \dot{\boldsymbol{F}}_i}\,, \tag{45}$$

where $\boldsymbol{F}_i \equiv \boldsymbol{F}(\overline{t}_i)$ and $\dot{\boldsymbol{F}}_i = \partial \boldsymbol{F}_i / \partial \overline{t}_i$. To an accuracy up to $\sim \Delta^3$, a trajectory satisfying the initial condition (21) has the form (25):

$$\boldsymbol{r}(t) = \boldsymbol{V}_i(\tau - i\Delta) - \frac{\boldsymbol{F}_i}{2}\left(\tau^2 + \Delta^2\right) - \frac{\dot{\boldsymbol{F}}_i}{6}(\tau^3 + i\Delta^3), \tag{46}$$

where $\tau = t - \overline{t}_i$ and

$$\boldsymbol{V}_i = \boldsymbol{K}_i + i\Delta \frac{\boldsymbol{K}_i}{t_f - \overline{t}_i} - \frac{\Delta^2}{2} \frac{\boldsymbol{K}_i}{(t_f - \overline{t}_i)^2} \approx \boldsymbol{K}_i e^{i \frac{\Delta}{t_f - \overline{t}_i}}. \tag{47}$$

In contrast to the case of ionization, $\boldsymbol{V}_i$ has a small imaginary part [cf. $\boldsymbol{V}_\nu$ (7)], which is not surprising, because $\boldsymbol{V}_i$ is not an observable. Since $\omega\Delta \ll 1$ and $t_f - \overline{t}_i \sim \omega^{-1}$, in practical calculations we can neglect the imaginary part of $\boldsymbol{V}_i$. Thus, the Coulomb factor is given by Eq. (31) with these substitutions: $\boldsymbol{F}_\nu \to \boldsymbol{F}_i$, $\boldsymbol{V}_\nu \to \boldsymbol{V}_i$, and $\mathcal{F}_\nu \to \mathcal{F}$.

According to Eq. (41a), for a one-dimensional (1D) field (e.g., a linearly polarized laser pulse or a multicolor field with components linearly polarized in the same direction), ionization events happen at instants for which $K_i = 0$, and thus the Coulomb factor coincides with the static one [see Eq. (32) with $F_\nu \to F_i$]. This result justifies the *ad hoc* generalization of the ionization factor for an electron in a short-range potential to that for an electron in an atom that was used in Refs. [42–44, 71].

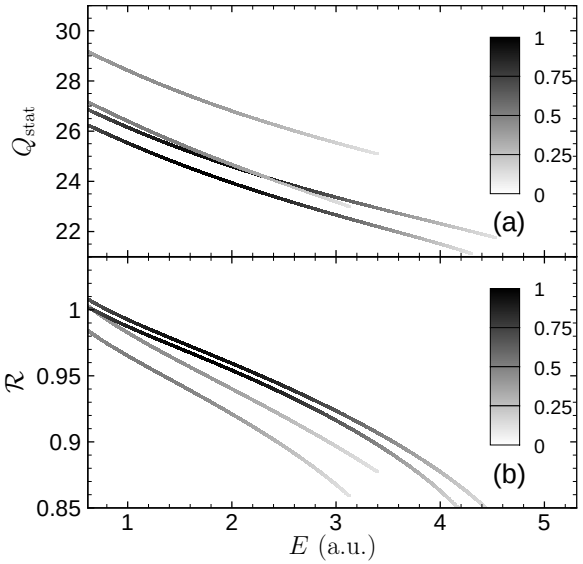


FIG. 5. Dependence on the harmonic energy ($E = \Omega - I_p$) of the Coulomb correction factors (a) $Q_{\rm stat}^{(\nu)}$ and (b) $\mathcal{R}^{(\nu)}$ for HHG in a bicircular laser field for each of the four most significant trajectories $\nu$. The color gradient of each curve shows the relative contribution of each trajectory $\nu$. Calculations were performed for $I_p = 13.65$ eV and for a bicircular field (48) with $\omega = 0.775$ eV, $I = 10^{14}$ W/cm$^2$, $N = 3$.

To test the accuracy of $Q_{\rm stat}$ for a more complicated 2D case, we calculate it for the case of HHG in a bicircular laser field. We parametrize the vector potential of the bicircular field (thus ensuring there is no DC component) as follows:

$$\boldsymbol{A}(t) = \boldsymbol{A}_1(t) + \boldsymbol{A}_2(t), \quad \boldsymbol{A}_i = \frac{\partial}{\partial t} \boldsymbol{R}_i(t), \tag{48}$$

$$\boldsymbol{R}_i = \frac{F_i}{\omega_i^2} e^{-2\ln 2 \frac{t^2}{\tau_i^2}} (\boldsymbol{e}_x \cos\omega_i t + \boldsymbol{e}_y \eta_i \sin\omega_i t), \tag{49}$$

where $\omega_1 = \omega$, $\omega_2 = 2\omega$, $F_1 = F_2 = F$, $\tau_1 = \tau_2 = 2\pi N/\omega$, and $\eta_1 = -\eta_2 = 1$. Our calculation is for an intensity $I = cF^2/(8\pi) = 10^{14}$ W/cm$^2$ and a wavelength $\lambda = 1.6\mu$m ($\hbar\omega = 0.775$ eV). The dependence of $Q_{\rm stat}^{(\nu)}$ and $\mathcal{R}^{(\nu)}$ [see Eqs. (31)–(33)] on the photoelectron energy $E$ at the instant of recombination is shown in Fig. 5 for each of the four most significant trajectories $\nu$. Our calculations show that the Coulomb factors decrease gradually with increasing harmonic energy. This fact is related to the increasing velocity $\boldsymbol{V}_i$ at the moment of ionization. We note that in the 2D case the Coulomb factor can be approximated with good accuracy by its static counterpart only in a narrow range of harmonic energies.

## VI. SUMMARY AND CONCLUSIONS

In this work we have derived general analytic expressions [see Eqs. (31)–(33)] for the Coulomb factor in the

probability amplitude for nonlinear ionization by a low-frequency intense laser field for the case in which the Keldysh parameter $\gamma$ is small. We have also presented detailed applications of our general formulas to the important special cases of LP and CP laser fields. Our analytic expressions, obtained in the adiabatic approximation, fill the need for reliable Coulomb correction factors in the gap between the static field (momentum-independent) Coulomb factor responsible for the enhancement of the total ionization rate [19, 55] and the one for arbitrary $\gamma$ and $\boldsymbol{p}$, which requires a demanding numerical calculation within the CCSFA or ARM methods. Application of our general formulas to the benchmarking cases of LP and CP fields shows that a noticeable dependence of the Coulomb factor on the photoelectron momentum survives even in the adiabatic limit.

The method developed in this paper has also allowed us to calculate the Coulomb factor in the probability for HHG. Here we predict that, in contrast to the case of a quasi-monochromatic LP pulse, the HHG spectrum in a bicircular laser field is rather strongly modified by the Coulomb interaction.

## ACKNOWLEDGMENTS

The authors gratefully acknowledge C. Blaga, L. DiMauro, and A. Rudenko for providing us with the experimental data appearing in our Fig. 4. This work was supported in part by the Ministry of Education and Science of the Russian Federation through Grant No. 3.1659.2017/4.6 and by the U.S. National Science Foundation (NSF) through Grant No. PHY-1505492 (A.F.S.). A collaborative visit to UNL by M.V.F. was supported in part by NSF EPSCoR IRR Track II Research Award No. 1430519. S.V.P. also acknowledges support from the MEPhI Academic Excellence Project (Contract No. 02.a03.21.0005).

## Appendix A: Strong field detachment probability in the adiabatic approximation

To specify momentum distribution for LP and CP fields, we consider a rectangular temporal envelope $f(t)$ for a laser pulse with an $N$-cycle flat part:

$$f(t)=\begin{cases}1, & 0\le t\le 2\pi N\\ 0, & \text{otherwise}\end{cases}.$$

For a LP laser field, $\boldsymbol{F}(t)=\boldsymbol{e}_z F f(t)\cos\omega t$, the real part of the saddle points in the adiabatic approximation is given by Eq. (16). Thus with this electric field we can calculate $S(\boldsymbol{p},\overline{t}_\nu)$ analytically:

$$S_+\equiv S\left(\boldsymbol{p},\overline{t}_\nu^{(+)}\right)=-\frac{3Fp_z}{4\omega^2}\sqrt{1-\left(\frac{p_z}{p_F}\right)^2}$$
$$+\frac{1}{\omega}\left(\frac{p^2}{2}+I_p+u_p\right)\left(\arcsin\frac{p_z}{p_F}+2\pi\nu\right), \quad \text{(A1a)}$$

$$S_-\equiv S\left(\boldsymbol{p},\overline{t}_\nu^{(-)}\right)=\frac{3Fp_z}{4\omega^2}\sqrt{1-\left(\frac{p_z}{p_F}\right)^2}$$
$$+\frac{1}{\omega}\left(\frac{p^2}{2}+I_p+u_p\right)\left(\pi-\arcsin\frac{p_z}{p_F}+2\pi\nu\right), \quad \text{(A1b)}$$

where $u_p=F^2/(4\omega^2)$. In order to calculate the detachment probability, we must specify $f_l(\boldsymbol{p},\overline{t}_\nu)$ in Eq. (13). For an initial $s$-state, the function $f_0(\boldsymbol{p},\overline{t}_\nu)$ has the form [37]:

$$f_0(\boldsymbol{p},\overline{t}_\nu^{(\pm)})=\frac{C_{\kappa\,0}}{2\pi}\sqrt{\frac{\kappa}{2}}, \quad \text{(A2)}$$

while for a $p$-state its form depends on the azimuthal quantum number $m$ [37]:

$$f_1(\boldsymbol{p},\overline{t}_\nu^{(\pm)})=\mp\frac{C_{\kappa\,1}}{2\pi}\sqrt{\frac{3\kappa}{2}\left[1+\left(\frac{p_\perp}{\kappa}\right)^2\right]},\ m=0, \quad \text{(A3)}$$

$$f_1(\boldsymbol{p},\overline{t}_\nu^{(\pm)})=-m\frac{C_{\kappa\,1}}{2\pi}\sqrt{\frac{3\kappa}{4}}\frac{p_\perp}{\kappa},\ m=\pm1, \quad \text{(A4)}$$

where $C_{\kappa\,l}$ is the dimensionless asymptotic coefficient of the bound state $\psi_0$:

$$\psi_0(\boldsymbol{r})|_{\kappa r\gg1}\approx\sqrt{\kappa}C_{\kappa\,l}\frac{e^{-\kappa r}}{r}Y_{l,m}(\hat{\boldsymbol{r}}).$$

Substituting Eqs. (17), (A1)-(A4) into (13), we obtain the detachment amplitude (3) in the form:

$$\mathcal{A}(\boldsymbol{p})=\frac{|f_l(\boldsymbol{p},\overline{t}_\nu^{\pm})|e^{-\frac{\varkappa_{\rm lin}^3}{3\mathcal{F}_{\rm lin}}+iS_++i\pi\alpha}}{\sqrt{2\pi\varkappa_{\rm lin}\mathcal{F}_{\rm lin}}}$$
$$\times\left[(-1)^l+e^{i(S_--S_+)}\right]\frac{\sin(2\pi N\alpha)}{\sin(\pi\alpha)}, \quad \text{(A5)}$$

where $l=0,1$ and $\alpha=(p^2/2+I_p+u_p)/\omega$. The differential (in $p_z$ and $p_\perp$) detachment probability is then found to be:

$$\frac{d^2\mathcal{P}(\boldsymbol{p})}{d\boldsymbol{p}}=|\mathcal{A}(\boldsymbol{p})|^2$$
$$=\frac{2l+1}{(2\pi)^3}C_{\kappa\,l}^2\frac{[1+(p_\perp/\kappa)^2]^{l-|m|-1/2}}{[1-(p_z/p_F)^2]^{1/2}F}\left(\frac{p_\perp}{2\kappa}\right)^{2|m|}e^{-\frac{2\varkappa_{\rm lin}^3}{3\mathcal{F}_{\rm lin}}}$$
$$\times\left[1+(-1)^{l+m}\cos(S_--S_+)\right]\left[\frac{\sin(2\pi N\alpha)}{\sin(\pi\alpha)}\right]^2. \quad \text{(A6)}$$

For large $N$ we can approximate:

$$\left[\frac{\sin(2\pi N\alpha)}{\sin(\pi\alpha)}\right]^2\approx2N\omega\sum_n\delta\left(\frac{p^2}{2}+I_p+u_p-n\omega\right)$$
$$=\frac{\mathcal{T}\omega^2}{2\pi}\sum_n\delta\left(\frac{p^2}{2}+I_p+u_p-n\omega\right), \quad \text{(A7)}$$

where $n$ is an integer number and $\mathcal{T} = 4\pi N/\omega$. We notice that the limiting case of a DC field can be obtained from (A6) by setting $N = 1/2$ and taking the limit $\omega \to 0$ and, hence, $p_F \to \infty$. In this case the third line of (A6) is equal 1, $\sqrt{1-(p_z/p_F)^2} \to 1$, $\varkappa_{\rm lin} \to \kappa$, and $\mathcal{F}_{\rm lin} \to F$.

For a CP field, $\boldsymbol{F}(t) = Ff(t)(\boldsymbol{e}_x \cos\omega t + \boldsymbol{e}_y \sin\omega t)$, the action $S(\boldsymbol{p}, \overline{t}_\nu)$ has a simple form:

$$S(\boldsymbol{p}, \overline{t}_\nu) = \left(\frac{p^2}{2} + I_p + 2u_p\right)\overline{t}_\nu. \tag{A8}$$

For the case of an initial $s$-state, the differential (in $p_{||}$ and $p_\perp$) detachment probability takes form:

$$\frac{d^2\mathcal{P}(\boldsymbol{p})}{d\boldsymbol{p}} = \frac{C^2_{\kappa\,0}}{2(2\pi)^3}\frac{\sqrt{p_F/p_{||}}}{F\overline{\varkappa}}\exp\left[-\frac{2\kappa^3}{F}\overline{\varkappa}^3\sqrt{\frac{p_F}{p_{||}}}\right] \times \left[\frac{\sin(2\pi N\overline{\alpha})}{\sin(\pi\overline{\alpha})}\right]^2, \tag{A9}$$

where $\overline{\alpha} = (p^2/2 + I_p + 2u_p)/\omega$ and

$$\overline{\varkappa} = \sqrt{1 + (p_\perp/\kappa)^2 + (p_{||} - p_F)^2/\kappa^2}. \tag{A10}$$

Near its maxima, $d^2\mathcal{P}(\boldsymbol{p})/d\boldsymbol{p}$ has a Gaussian distribution that is independent of the angle $\varphi$ and has cylindrical symmetry with respect to the axis perpendicular to the polarization plane [36, 37].


[1] F.H.M. Faisal, "Strong-field physics: Ionization surprise," Nat. Phys. **5**, 319 (2009).

[2] C.I. Blaga, F. Catoire, P. Colosimo, G.G. Paulus, H.G. Muller, P. Agostini, and L.F. DiMauro, "Strong-field photoionization revisited," Nat. Phys. **5**, 335 (2009).

[3] W. Quan, Z. Lin, M. Wu, H. Kang, H. Liu, X. Liu, J. Chen, J. Liu, X.T. He, S.G. Chen, H. Xiong, L. Guo, H. Xu, Y. Fu, Y. Cheng, and Z.Z. Xu, "Classical aspects in above-threshold ionization with a midinfrared strong laser field," Phys. Rev. Lett. **103**, 093001 (2009).

[4] C.Y. Wu, Y.D. Yang, Y.Q. Liu, Q.H. Gong, M. Wu, X. Liu, X.L. Hao, W.D. Li, X.T. He, and J. Chen, "Characteristic spectrum of very low-energy photoelectron from above-threshold ionization in the tunneling regime," Phys. Rev. Lett. **109**, 043001 (2012).

[5] J. Dura, N. Camus, A. Thai, A. Britz, M. Hemmer, M. Baudisch, A. Senftleben, C.D. Schröter, J. Ullrich, R. Moshammer, and J. Biegert, "Ionization with low-frequency fields in the tunneling regime," Sci. Rep. **3**, 2675 (2013).

[6] Y. Huismans, A. Rouzée, A. Gijsbertsen, J.H. Jungmann, A.S. Smolkowska, P.S. W.M. Logman, F. Lépine, C. Cauchy, S. Zamith, T. Marchenko, J.M. Bakker, G. Berden, B. Redlich, A.F.G. van der Meer, H.G. Muller, W. Vermin, K.J. Schafer, M. Spanner, M.Yu. Ivanov, O. Smirnova, D. Bauer, S.V. Popruzhenko, and M.J.J. Vrakking, "Time-resolved holography with photoelectrons," Science **331**, 61 (2011).

[7] Th. Keil, S.V. Popruzhenko, and D. Bauer, "Laser-driven recollisions under the Coulomb barrier," Phys. Rev. Lett. **117**, 243003 (2016).

[8] M.-C. Chen, P. Arpin, T. Popmintchev, M. Gerrity, B. Zhang, M. Seaberg, D. Popmintchev, M.M. Murnane, and H.C. Kapteyn, "Bright, coherent, ultrafast soft X-ray harmonics spanning the water window from a tabletop light source," Phys. Rev. Lett. **105**, 173901 (2010).

[9] T. Popmintchev, M.-C. Chen, P. Arpin, M.M. Murnane, and H.C. Kapteyn, "The attosecond nonlinear optics of bright coherent X-ray generation," Nat. Phot. **4**, 822 (2010).

[10] M.-C. Chen, C. Mancuso, C. Hernández-García, F. Dollar, B. Galloway, D. Popmintchev, P.-C. Huang, B. Walker, L. Plaja, A.A. Jaroń-Becker, A. Becker, M.M. Murnane, H.C. Kapteyn, and T. Popmintchev, "Generation of bright isolated attosecond soft x-ray pulses driven by multicycle midinfrared lasers," Proc. Natl. Acad. Sci. USA **111**, E2361 (2014).

[11] F. Krausz and M. Ivanov, "Attosecond physics," Rev. Mod. Phys. **81**, 163 (2009).

[12] V.S. Popov, "Tunnel and multiphoton ionization of atoms and ions in a strong laser field (Keldysh theory)," Usp. Fiz. Nauk **174**, 921 (2004) [Sov. Phys. — Physics–Uspekhi **47**, 855 (2004)].

[13] D.B. Milošević, G.G. Paulus, D. Bauer, and W. Becker, "Above-threshold ionization by few-cycle pulses," J. Phys. B **39**, R203 (2006).

[14] S.V. Popruzhenko, "Keldysh theory of strong field ionization: history, applications, difficulties and perspectives," J. Phys. B **47**, 204001 (2014).

[15] B.M. Karnakov, V.D. Mur, S.V. Popruzhenko, and V.S. Popov, "Current progress in developing the nonlinear ionization theory of atoms and ions," Usp. Fiz. Nauk **185**, 3 (2015) [Sov. Phys. — Physics–Uspekhi **58**, 3 (2015)].

[16] M. Lewenstein, Ph. Balcou, M.Yu. Ivanov, A. L'Huillier, and P.B. Corkum, "Theory of high-harmonic generation by low-frequency laser fields," Phys. Rev. A **49**, 2117 (1994).

[17] S.V. Popruzhenko and D. Bauer, "Strong field approximation for systems with Coulomb interaction," J. Mod. Opt. **55**, 2573 (2008).

[18] L.V. Keldysh, "Ionization in the field of a strong electromagnetic wave," Zh. Eksp. Teor. Fiz. **47**, 1945 (1964) [Sov. Phys.–JETP **20**, 1307 (1965)].

[19] A.M. Perelomov and V.S. Popov, Zh. Eksp. Teor. Fiz. **52**, 514 (1967) [Sov. Phys.–JETP **25**, 336 (1967)].

[20] B.M. Smirnov and M.I. Chibisov, "The breaking up of atomic particles by an electric field and by electron collisions," Zh. Eksp. Teor. Fiz. **49**, 841 (1965) [Sov. Phys.–JETP **22**, 585 (1966)].

[21] O. Kfir, P. Grychtol, E. Turgut, R. Knut, D. Zusin, D. Popmintchev, T. Popmintchev, H. Nembach, J.M. Shaw, A. Fleischer, H. Kapteyn, M. Murnane, and O. Cohen, "Generation of bright phase-matched circularly-polarized extreme ultraviolet high harmonics,"

Nat. Phot. **9**, 99 (2015).
[22] T. Fan, P. Grychtol, R. Knut, C. Hernández-García, D.D. Hickstein, D. Zusin, C. Gentry, F.J. Dollar, C.A. Mancuso, C.W. Hogle, O. Kfir, D. Legut, K. Carva, J.L. Ellis, K.M. Dorney, C. Chen, O.G. Shpyrko, E.E. Fullerton, O. Cohen, P.M. Oppeneer, D.B. Milošević, A. Becker, A.A. Jaroń-Becker, T. Popmintchev, M.M. Murnane, and H.C. Kapteyn, "Bright circularly polarized soft x-ray high harmonics for x-ray magnetic circular dichroism," Proc. Natl. Acad. Sci. USA **112**, 14206 (2015).
[23] C. Chen, Z. Tao, C. Hernández-García, P. Matyba, A. Carr, R. Knut, O. Kfir, D. Zusin, C. Gentry, P. Grychtol, O. Cohen, L. Plaja, A. Becker, A. Jaron-Becker, H. Kapteyn, and M. Murnane, "Tomographic reconstruction of circularly polarized high-harmonic fields: 3D attosecond metrology," Sci. Adv. **2**, e1501333 (2016).
[24] D.B. Milošević, "Generation of elliptically polarized attosecond pulse trains," Opt. Lett. **40**, 2381 (2015).
[25] L. Medišauskas, J. Wragg, H. van der Hart, and M.Yu. Ivanov, "Generating isolated elliptically polarized attosecond pulses using bichromatic counterrotating circularly polarized laser fields," Phys. Rev. Lett. **115**, 153001 (2015).
[26] D.B. Milošević, "Circularly polarized high harmonics generated by a bicircular field from inert atomic gases in the $p$ state: A tool for exploring chirality-sensitive processes," Phys. Rev. A **92**, 043827 (2015).
[27] D. Baykusheva, M.S. Ahsan, N. Lin, and H.J. Wörner, "Bicircular high-harmonic spectroscopy reveals dynamical symmetries of atoms and molecules," Phys. Rev. Lett. **116**, 123001 (2016).
[28] N.L. Manakov, M.V. Frolov, B. Borca, and A.F. Starace, "Multiphoton detachment of a negative ion by an elliptically polarized, monochromatic laser field," J. Phys. B **36**, R49 (2003).
[29] O.I. Tolstikhin, T. Morishita, and S. Watanabe, "Adiabatic theory of ionization of atoms by intense laser pulses: One-dimensional zero-range-potential model," Phys. Rev. A **81**, 033415 (2010).
[30] Y. Okajima, O.I. Tolstikhin, and T. Morishita, "Adiabatic theory of high-order harmonic generation: One-dimensional zero-range-potential model," Phys. Rev. A **85**, 063406 (2012).
[31] O.I. Tolstikhin and T. Morishita, "Adiabatic theory of ionization by intense laser pulses: Finite-range potentials," Phys. Rev. A **86**, 043417 (2012).
[32] W. Becker, F. Grasbon, R. Kopold, D.B. Milošević, G.G. Paulus, and H. Walther, "Above threshold ionization: From classical features to quantum effects," Adv. At. Mol. Opt. Phys. **48**, 35 (2002).
[33] D.B. Milošević and F. Ehlotzky, "Scattering and reaction processes in powerfull laser fields," Adv. At. Mol. Opt. Phys. **49**, 373 (2003).
[34] A. Becker and F.H.M. Faisal, "Intense-field many-body S-matrix theory," J. Phys. B **38**, R1 (2005).
[35] W. Becker, J. Chen, S.G. Chen, and D.B. Milošević, "Dressed-state strong-field approximation for laser-induced molecular ionization," Phys. Rev. A **76**, 033403 (2007).
[36] A.I. Nikishov and V.I. Ritus, "Ionization of systems bound by short-range forces by the field of an electromagnetic wave," Zh. Eksp. Teor. Fiz. **50**, 255 (1966) [Sov. Phys.–JETP **23**, 168 (1966)].
[37] A.M. Perelomov, V.S. Popov, and M.V. Terentev, "Ionization of atoms in an alternating electric field," Zh. Eksp. Teor. Fiz. **50**, 1393 (1966) [Sov. Phys.–JETP **23**, 924 (1966)].
[38] F.H.M. Faisal, "Multiple absorption of laser photons by atoms," J. Phys. B **6**, L89 (1973).
[39] H.R. Reiss, "Effect of an intense electromagnetic field on a weakly bound system," Phys. Rev. A **22**, 1786 (1980).
[40] P.B. Corkum, "Plasma perspective on strong-field multiphoton ionization," Phys. Rev. Lett. **71**, 1994 (1993).
[41] M.V. Frolov, N.L. Manakov, E.A. Pronin, and A.F. Starace, "Model-independent quantum approach for intense laser detachment of a weakly-bound electron," Phys. Rev. Lett. **91**, 053003 (2003).
[42] M.V. Frolov, N.L. Manakov, T.S. Sarantseva, M.Yu. Emelin, M.Yu. Ryabikin, and A.F. Starace, "Analytic description of the high-energy plateau in harmonic generation by atoms: Can the harmonic power increase with increasing laser wavelengths?" Phys. Rev. Lett. **102**, 243901 (2009).
[43] M.V. Frolov, N.L. Manakov, A.A. Silaev, and N.V. Vvedenskii, "Analytic description of high-order harmonic generation by atoms in a two-color laser field," Phys. Rev. A **81**, 063407 (2010).
[44] M.V. Frolov, N.L. Manakov, A.M. Popov, O.V. Tikhonova, E.A. Volkova, A.A. Silaev, N.V. Vvedenskii, and A.F. Starace, "Analytic theory of high-order harmonic generation by an intense few-cycle laser pulse," Phys. Rev. A **85**, 033416 (2012).
[45] M.V. Frolov, D.V. Knyazeva, N.L. Manakov, A.M. Popov, O.V. Tikhonova, E.A. Volkova, M.-H. Xu, L.-Y. Peng, L.-W. Pi, and A.F. Starace, "Validity of factorization of the high-energy photoelectron yield in above-threshold ionization of an atom by a short laser pulse," Phys. Rev. Lett. **108**, 213002 (2012).
[46] M.V. Frolov, D.V. Knyazeva, N.L. Manakov, J.-W. Geng, L.-Y. Peng, and A.F. Starace, "Analytic model for the description of above-threshold ionization by an intense short laser pulse," Phys. Rev. A **89**, 063419 (2014).
[47] W. Gordon, "The Compton effect according to Schrödinger's theory," Z. Phys. **40**, 117 (1926).
[48] D.M. Wolkow, "Über eine Klasse von Lösungen der Diracschen Gleichung," Z. Phys. **94**, 250 (1935).
[49] D.M. Volkov, "Electron in the field of plane unpolarized electromagnetic waves from the standpoint of the Dirac equation," Zh. Exp. Teor. Fiz. **7**, 1286 (1937).
[50] V.B. Berestetskii, E.M. Lifshitz, and L.P. Pitaevskii, *Quantum Electrodynamics* (Pergamon, Oxford, 1982).
[51] V.S. Popov, "Imaginary-time method in quantum mechanics and field theory," Phys. At. Nucl. **68**, 686 (2005).
[52] O. Smirnova, M. Spanner, and M. Ivanov, "Anatomy of strong field ionization II: to dress or not to dress?" J. Mod. Opt. **54**, 1019 (2007).
[53] L. Torlina and O. Smirnova, "Time-dependent analytical R-matrix approach for strong-field dynamics. I. One-electron systems," Phys. Rev. A **86**, 043408 (2012).
[54] S.V. Popruzhenko, G.G. Paulus, and D. Bauer, "Coulomb-corrected quantum trajectories in strong-field ionization," Phys. Rev. A **77**, 053409 (2008).
[55] S.V. Popruzhenko, V.D. Mur, V.S. Popov, and D. Bauer, "Strong field ionization rate for arbitrary laser frequencies," Phys. Rev. Lett. **101**, 193003 (2008).
[56] T.-M. Yan, S.V. Popruzhenko, M.J.J. Vrakking, and D. Bauer, "Low-energy structures in strong field ioniza-

tion revealed by quantum orbits," Phys. Rev. Lett. **105**, 253002 (2010).

[57] L. Torlina, F. Morales, J. Kaushal, I. Ivanov, A. Kheifets, A. Zielinski, A. Scrinzi, H.G. Muller, S. Sukiasyan, M. Ivanov, and O. Smirnova, "Interpreting attoclock measurements of tunnelling times," Nat. Phys. **11**, 503 (2015).

[58] L. Torlina and O. Smirnova, "Coulomb time delays in high harmonic generation," New J. Phys. **19**, 023012 (2017).

[59] S.V. Popruzhenko, "Invariant form of Coulomb corrections in the theory of nonlinear ionization of atoms by intense laser radiation," Zh. Eksp. Teor. Fiz. **145**, 664 (2014) [Sov. Phys.–JETP **118**, 580 (2014)].

[60] E. Pisanty and M. Ivanov, "Slalom in complex time: Emergence of low-energy structures in tunnel ionization via complex-time contours," Phys. Rev. A **93**, 043408 (2016).

[61] C. Liu and K.Z. Hatsagortsyan, "Origin of unexpected low energy structure in photoelectron spectra induced by midinfrared strong laser fields," Phys. Rev. Lett. **105**, 113003 (2010).

[62] N.I. Shvetsov-Shilovski, M. Lein, L.B. Madsen, E. Räsänen, C. Lemell, J. Burgdörfer, D.G. Arbó, and K. Tőkési, "Semiclassical two-step model for strong-field ionization," Phys. Rev. A **94**, 013415 (2016).

[63] T.-M. Yan and D. Bauer, "Sub-barrier coulomb effects on the interference pattern in tunneling-ionization photoelectron spectra," Phys. Rev. A **86**, 053403 (2012).

[64] L.D. Landau and E.M. Lifshitz, *Quantum Mechanics (Nonrelativistic Theory)* (Pergamon, Oxford, 1977).

[65] S.P. Goreslavskii and S.V. Popruzhenko, "Differential photoelectron distributions in a strong elliptically polarized low-frequency laser field," Zh. Eksp. Teor. Fiz. **110**, 1200 (1996) [Sov. Phys.–JETP **83**, 661 (1996)].

[66] V.D. Mur, S.V. Popruzhenko, and V.S. Popov, "Energy and momentum spectra of photoelectrons under conditions of ionization by strong laser radiation (The case of elliptic polarization)," Zh. Eksp. Teor. Fiz. **119**, 893 (2001) [Sov. Phys.–JETP **92**, 777 (2001)].

[67] Yu.A. Brychkov, O.I. Marichev, and A.P. Prudnikov, *Integraly i riady. Elementarnye funktsii* (Moskva: Fizmatlit, 2002).

[68] G.G. Paulus, W. Becker, W. Nicklich, and H. Walther, "Rescattering effects in above-threshold ionization: a classical model," J. Phys. B **27**, L703 (1994).

[69] P.B. Corkum and F. Krausz, "Attosecond science," Nat. Phys. **3**, 381 (2007).

[70] A.A. Minina, M.V. Frolov, A.N. Zheltukhin, and N.V. Vvedenskii, "Tunnelling approximation for estimating the amplitude of high harmonic generation in intense laser fields: analysis of ionisation and recombination times," Quant. Elect. **47**, 216 (2017).

[71] M.V. Frolov, N.L. Manakov, A.A. Silaev, N.V. Vvedenskii, and A.F. Starace, "High-order harmonic generation by atoms in a few-cycle laser pulse: Carrier-envelope phase and many-electron effects," Phys. Rev. A **83**, 021405(R) (2011).

[72] A. Rudenko, K. Zrost, C.D. Schröter, V.L.B. de Jesus, B. Feuerstein, R. Moshammer and J. Ullrich, "Resonant structures in the low-energy electron continuum for single ionization of atoms in the tunnelling regime," J. Phys. B **37** L407 (2004).

[73] A. Kästner, U. Saalmann and J.M. Rost, "Electron-Energy Bunching in Laser-Driven Soft Recollisions," Phys. Rev. Lett. **108**, 033201 (2012).